The Solar Flare 4 – 10 keV X-ray Spectrum

K. J. H. Phillips

National Research Council Senior Research Associate, NASA Goddard Space Flight Center,

Greenbelt, MD 20771

phillips@stars.gsfc.nasa.gov

Received _____; accepted _____

Submitted to Astrophysical Journal

ABSTRACT

The 4–10 keV solar flare spectrum includes highly excited lines of stripped Ca, Fe, and Ni ions as well as a continuum steeply falling with energy. Groups of lines at $\sim$ 7 keV and $\sim$ 8 keV, observed during flares by the broad-band *RHESSI* spectrometer and called here the Fe-line and Fe/Ni-line features, are formed mostly of Fe lines but with Ni lines contributing to the $\sim$ 8 keV feature. Possible temperature indicators of these line features are discussed – the peak or centroid energies of the Fe-line feature, the line ratio of the Fe-line to the Fe/Ni-line features, and the equivalent width of the Fe-line feature. The equivalent width is by far the most sensitive to temperature. However, results will be confused if, as is commonly believed, the abundance of Fe varies from flare to flare, even during the course of a single flare. With temperature determined from the thermal continuum, the Fe-line feature becomes a diagnostic of the Fe abundance in flare plasmas. These results are of interest for other hot plasmas in coronal ionization equilibrium such as stellar flare plasmas, hot gas in galaxies, and older supernova remnants.

Subject headings: Sun: flares—Sun: X-rays, gamma rays

1. Introduction

The region 3.8–10 keV (λ 1.2–3.3 Å) in solar-flare X-ray spectra is of great importance in inferring the properties of the hottest parts of the thermal plasma created during a solar flare. It contains emission lines of highly ionized Ca, Fe, and Ni atoms, and a continuum which falls off steeply with increasing energy. Spectra covering this region with broad-band energy resolution (FWHM 0.2–0.8 keV) were obtained by the Soft X-ray

Spectrometer part of the Wide Band Spectrometer on *Yohkoh* (Yoshimori et al. 1991) and the solid-state PIN detector, part of the X-ray/gamma-ray spectrometer (XGRS) aboard the *Near Earth Asteroid Rendezvous* (*NEAR*) mission (Starr et al. 2000). Most recently, the nine germanium detectors making up the *Reuven Ramaty High Energy Solar Spectroscopic Imager* (*RHESSI*: Lin et al. (2002)), launched in February 2002 and continuing to operate at the present time, are observing the solar flare spectrum in the range 3 keV–17 MeV; the spectral resolution in the range 3–10 keV is as high as $\sim$ 0.8 keV (FWHM). During the flare impulsive stage, a nonthermal continuum is often evident in *RHESSI* spectra at $E \gtrsim 20$ keV, decreasing much less steeply with E than the thermal continuum, and having a power-law dependence (intensity $\propto E^{-\gamma}$). This component is commonly attributed to bremsstrahlung emitted by beamed nonthermal electrons as they travel downwards from near the apex of a magnetic loop and lose their energy in the chromosphere or lower corona by Coulomb collisions. Images from *RHESSI* and the HXT and SXT instruments on the *Yohkoh* spacecraft indicate that the nonthermal bremsstrahlung originates at flare loop footpoints and the thermal plasma is located near or slightly above the loop apex (Lin et al. 2002; Masuda 1994).

The thermal component in *RHESSI* and *NEAR*-PIN spectra is observed to have a prominent broadened emission line feature at 7 keV and a less intense line feature at 8 keV indicating high plasma temperatures. The 7 keV feature corresponds to two groups of emission lines, due to Fe XXV $1s^2 - 1s2l$ ($l = s, p$) lines and associated dielectronic satellites and centered on $\sim$ 6.6 keV, and to Fe XXVI $1s - 2p$ (Lyα) lines and associated satellites, centered on $\sim$ 6.9 keV. The Fe XXV lines are excited at electron temperatures $T_e \gtrsim 12$ MK, while the Fe XXVI lines are excited at $T_e \gtrsim 30$ MK. This line complex is referred to here as the Fe-line feature. The 8 keV line feature corresponds to Fe XXV $1s^2 - 1snp$ ($n \geq 3$) lines and Fe XXVI $1s - np$ ($n \geq 3$) lines as well as Ni XXVII $1s^2 - 1s2p$ and Ni XXVIII $1s - 2p$ lines. This will be referred to as the Fe/Ni-line feature. Unlike the lines making up

the Fe-line feature which have been widely observed, hardly any high-resolution spectra – solar, non-solar, or laboratory – exist showing the lines making up the Fe/Ni-line feature, so *RHESSI* and *NEAR*-PIN solar flare observations of the Fe/Ni line feature give unique information about these lines which have the highest excitation energies in the X-ray spectrum.

RHESSI observations of the Fe-line and Fe/Ni-line features, together with those of the thermal continuum, now being routinely made during flares, provide valuable tools in finding T_e and the iron abundance ($A_{\rm flare}({\rm Fe}) = N({\rm Fe})/N({\rm H})$) in flare plasmas. This paper describes the diagnostic capability of these line features which can be applied to solar flares and non-solar X-ray sources with similar excitation conditions.

2. Line Emission in the 3.8–10 keV Range

2.1. Principal Lines and their Excitation

The main ions represented in flare 3.8–10-keV spectra are H-like or He-like Ca, Fe, and Ni ions. (Several Ar and S lines occur between 3.0 and 3.8 keV which the *RHESSI* energy range extends down to, but we shall not consider them here.) An early crystal spectrometer observation during a large flare (Neupert & Swartz 1970) also shows weak lines due to He-like Ti, Cr, and Mn ions. The thermal component of most solar flares have $T_e < 30$ MK, when the He-like Ca lines (3.86–3.90 keV) and He-like Fe lines and satellites (6.4–6.7 keV) are the most intense. The resonance lines (w in the notation of Gabriel (1972)) of Ca XIX, Fe XXV, and Ni XXVII are due to $1s^2\,{}^1S_0 - 1s2p\,{}^1P_1$ transitions. Intercombination and forbidden lines also occur, on the low-energy side of each w line; their transitions are (in decreasing energy) $1s^2\,{}^1S_0 - 1s2p\,{}^3P_{1,2}$ (lines y, x) and $1s^2\,{}^1S_0 - 1s2s\,{}^3S_1$ (line z). Higher-excitation lines with transitions $1s^2\,{}^1S_0 - 1snp\,{}^1P_1$ ($n \geq 3$) occur at progressively

higher energies and decreasing intensities. Lyman-series lines emitted by H-like Ca, Fe, and Ni also occur in this range. The Fe XXVI Lyα lines, for example, are weak at $T_e < 30$ MK but are comparable in intensity to Fe XXV line w at $T_e \gtrsim 80$ MK.

Satellite lines occur on the low-energy side of the H-like and He-like ion resonance lines. Those near the He-like ion lines are due to $1s^2nl - 1s2pnl$ ($n \geq 2$, $l = s$, p etc.) in Li-like ions and equivalent transitions in lower ionization stages. The doubly excited $1s2pnl$ states are formed by dielectronic recombination or (for some $n = 2$ satellites) inner-shell excitation. Satellites with transitions $1s^2\,nl - 1s2pnl$ ($n \geq 4$) are less and less separated from Fe XXV line w for increasing n. The most intense $n = 2$ Li-like ion satellites are labelled a, j, k ($1s^22p - 1s2p^2$ transitions), q, r, s, and t ($1s^22s - 1s2s2p$ transitions), and $d13/d15$ ($1s^23p - 1s2p3p$). Satellites emitted by Be-like to C-like ions (transitions $1s^22s^22p^n - 1s2s^22p^{n+1}$) occur in groups for each ionization stage. Thus, Fe XXIII–Fe XIX lines occur in energy intervals of ~ 0.03 keV at progressively smaller energies down to 6.47 keV (Phillips et al. 1983). Lower ionization stages are represented by pairs of lines that for ions with only a few missing electrons are unresolvable from the Fe II $1s - 2p$ lines forming the Kα doublet at 6.400, 6.387 keV. Similarly, He-like ion satellite lines with transitions $1s2l - 2l2l'$ ($l, l' = s$, p) occur on the low-energy side of either of the Lyα lines. Several satellites (most intense being $1s2p\,^1P_1 - 2p^2\,^1D_2$) coincide to form a single intense line feature known as J (Doschek et al. 1979; Dubau et al. 1981).

A few lines are formed by fluorescence of the photosphere by the soft X-ray thermal plasma in the corona. They are emitted when one of the two $1s$ electrons in neutral or once-ionized Fe and Ni atoms in the photosphere is removed by photons with energies greater than the K-shell binding energy I_K (7.11 keV for Fe, 8.33 keV for Ni), followed by a radiative transition from the $2p$ or $3p$ shell (Kα, Kβ lines, respectively). De-excitation may also proceed by re-arrangement of the atom and emission of an Auger electron.

The fluorescence yield (relative probability of the radiative transition) ω_K increases approximately as Z^4 (Z = atomic number) so is much greater for Fe and Ni than for lighter elements. Free electrons with energies $> I_K$, such as are present in the flare impulsive stage, may also K-shell-ionize these atoms (Phillips & Neupert 1973) but flare observations show that fluorescence dominates (Bai 1979; Parmar et al. 1984; Emslie et al. 1986; Phillips et al. 1994).

High-resolution ($E/\Delta E \gtrsim 4000$) solar flare spectra covering the H-like and He-like Ca and Fe $n = 1 - 2$ lines and lower ionization stages have been obtained with curved Bragg crystal spectrometers aboard *P78-1* (Doschek et al. 1980), *Solar Maximum Mission* (Acton et al. 1980), *Hinotori* (Tanaka 1986), *Yohkoh* (Culhane et al. 1991), and *Coronas-F* (Sylwester et al. 2002). High-resolution He-like Fe and Ni spectra from tokamak plasmas were obtained, with curved crystal spectrometers, by Bitter et al. (1979), Bombarda et al. (1988), and Bitter et al. (1991). Generally these spectrometers had small energy ranges that included only the lines of interest, e.g. the *Yohkoh* spectrometer observed only the Ca XIX w and x lines, the Fe XXV lines $w - z$ and satellites, and the Fe XXVI Lyα lines.

In Table 1 we give details of the principal lines in the range 3.859–10.342 keV. Their relative importance is indicated by calculated intensities from the Chianti code (Dere et al. 1997) at two temperatures, 20 MK (typical of a solar flare) and 100 MK (observed in some non-solar sources).

2.2. Lines making up the Fe-line and Fe/Ni-line Features

We now discuss the individual lines making up the Fe-line and Fe/Ni-line features and their contribution functions, i.e. the dependence on T_e of their emission per unit emission measure $\int_V N_e^2 dV$ (N_e = electron density, V = source volume). The Fe-line feature is here

also from Bely-Dubau et al. (1982).

Satellite lines formed by dielectronic recombination (e.g. j) have intensities (Gabriel 1972; Bely-Dubau et al. 1982)

$$I_s = \frac{N(\mathrm{Fe}^{+24})N_e V}{4\pi(1\mathrm{AU})^2} \times \frac{2.07 \times 10^{-16}\, F_s}{T_e^{3/2}} \times \exp(-E_s/k_B T_e) \qquad \text{photons cm}^{-2}\text{s}^{-1} \qquad (2)$$

where F_s is given by

$$F_s = \frac{g_s\, A_r\, A_a}{A_a + \Sigma A_r}, \qquad (3)$$

g_s being the statistical weight of the satellite's lower level, A_r the radiative transition rate from the satellite's doubly excited upper level, A_a the corresponding auto-ionization rate, ΣA_r the sum of all possible radiative transition rates from the upper level, and E_s the satellite's transition energy. Values of I_s were calculated for j and other satellites using the atomic data of Bely-Dubau et al. (1979), Bely-Dubau et al. (1982), and Lemen et al. (1984).

The inner-shell $n = 2$ satellites (e.g. q) have intensities given by

$$I'_s = \frac{N(\mathrm{Fe}^{+23})N_e V}{4\pi(1\mathrm{AU})^2} \times \frac{8.63 \times 10^{-6}\, \Upsilon_s \exp(-E_s/k_B T_e)}{T_e^{1/2}} \qquad \text{photons cm}^{-2}\text{s}^{-1} \qquad (4)$$

where $N(\mathrm{Fe}^{+23})$ is the number density of Fe^{+23} ions ($= N(\mathrm{Fe}^{+23})/N(\mathrm{Fe}) \times A_{\mathrm{flare}}(\mathrm{Fe})$) and Υ_s is the temperature-averaged collision strength of the satellite line transition. There is hence a T_e-dependence through the ionization fraction $N(\mathrm{Fe}^{+23})/N(\mathrm{Fe}^{+24})$. Values of I'_s were calculated using data of Lemen et al. (1984) and ionization fractions of Mazzotta et al. (1998).

higher energies and decreasing intensities. Lyman-series lines emitted by H-like Ca, Fe, and Ni also occur in this range. The Fe XXVI Lyα lines, for example, are weak at $T_e < 30$ MK but are comparable in intensity to Fe XXV line w at $T_e \gtrsim 80$ MK.

Satellite lines occur on the low-energy side of the H-like and He-like ion resonance lines. Those near the He-like ion lines are due to $1s^2nl - 1s2pnl$ ($n \geq 2$, $l = s$, p etc.) in Li-like ions and equivalent transitions in lower ionization stages. The doubly excited $1s2pnl$ states are formed by dielectronic recombination or (for some $n = 2$ satellites) inner-shell excitation. Satellites with transitions $1s^2nl - 1s2pnl$ ($n \geq 4$) are less and less separated from Fe XXV line w for increasing n. The most intense $n = 2$ Li-like ion satellites are labelled a, j, k ($1s^22p - 1s2p^2$ transitions), q, r, s, and t ($1s^22s - 1s2s2p$ transitions), and $d13/d15$ ($1s^23p - 1s2p3p$). Satellites emitted by Be-like to C-like ions (transitions $1s^22s^22p^n - 1s2s^22p^{n+1}$) occur in groups for each ionization stage. Thus, Fe XXIII–Fe XIX lines occur in energy intervals of ~ 0.03 keV at progressively smaller energies down to 6.47 keV (Phillips et al. 1983). Lower ionization stages are represented by pairs of lines that for ions with only a few missing electrons are unresolvable from the Fe II $1s - 2p$ lines forming the Kα doublet at 6.400, 6.387 keV. Similarly, He-like ion satellite lines with transitions $1s2l - 2l2l'$ ($l, l' = s$, p) occur on the low-energy side of either of the Lyα lines. Several satellites (most intense being $1s2p\,^1P_1 - 2p^2\,^1D_2$) coincide to form a single intense line feature known as J (Doschek et al. 1979; Dubau et al. 1981).

A few lines are formed by fluorescence of the photosphere by the soft X-ray thermal plasma in the corona. They are emitted when one of the two $1s$ electrons in neutral or once-ionized Fe and Ni atoms in the photosphere is removed by photons with energies greater than the K-shell binding energy I_K (7.11 keV for Fe, 8.33 keV for Ni), followed by a radiative transition from the $2p$ or $3p$ shell (Kα, Kβ lines, respectively). De-excitation may also proceed by re-arrangement of the atom and emission of an Auger electron.

The fluorescence yield (relative probability of the radiative transition) ω_K increases approximately as Z^4 (Z = atomic number) so is much greater for Fe and Ni than for lighter elements. Free electrons with energies $> I_K$, such as are present in the flare impulsive stage, may also K-shell-ionize these atoms (Phillips & Neupert 1973) but flare observations show that fluorescence dominates (Bai 1979; Parmar et al. 1984; Emslie et al. 1986; Phillips et al. 1994).

High-resolution ($E/\Delta E \gtrsim 4000$) solar flare spectra covering the H-like and He-like Ca and Fe $n = 1 - 2$ lines and lower ionization stages have been obtained with curved Bragg crystal spectrometers aboard *P78-1* (Doschek et al. 1980), *Solar Maximum Mission* (Acton et al. 1980), *Hinotori* (Tanaka 1986), *Yohkoh* (Culhane et al. 1991), and *Coronas-F* (Sylwester et al. 2002). High-resolution He-like Fe and Ni spectra from tokamak plasmas were obtained, with curved crystal spectrometers, by Bitter et al. (1979), Bombarda et al. (1988), and Bitter et al. (1991). Generally these spectrometers had small energy ranges that included only the lines of interest, e.g. the *Yohkoh* spectrometer observed only the Ca XIX w and x lines, the Fe XXV lines $w - z$ and satellites, and the Fe XXVI Lyα lines.

In Table 1 we give details of the principal lines in the range 3.859–10.342 keV. Their relative importance is indicated by calculated intensities from the Chianti code (Dere et al. 1997) at two temperatures, 20 MK (typical of a solar flare) and 100 MK (observed in some non-solar sources).

2.2. Lines making up the Fe-line and Fe/Ni-line Features

We now discuss the individual lines making up the Fe-line and Fe/Ni-line features and their contribution functions, i.e. the dependence on T_e of their emission per unit emission measure $\int_V N_e^2 dV$ (N_e = electron density, V = source volume). The Fe-line feature is here

defined as the excess above the continuum, as observed by a spectrometer with resolution FWHM $\approx$ 0.8 keV, in the range 5.8–7.5 keV, the Fe/Ni-line feature in the range 7.5–9.2 keV. We calculate the contribution functions in the form of fluxes (photons cm^{-2} s^{-1}) at the distance of the Earth (1 AU = 1.5×10^{13} cm) for an emission measure of 10^{49} cm^{-3}. Note that we take ion temperatures $T_{\rm ion}$ to be equal to T_e on the basis that equilibration times for a wide range of conditions ($T_e = 10 - 50$ MK, $N_e \gtrsim 3 \times 10^{10}$ cm^{-3}) are less than 10 s (Spitzer 1962), i.e. less than the time scale of thermal component of most flares.

Fe XXV line w (6.696 keV) is the most intense single line in the energy range of the Fe line feature for a wide range of T_e. The line emission is almost entirely due to direct collisional excitation from the ground state, with a small proportion (ϵ) due to cascades, unresolved dielectronic satellites, and excitation by recombination from H-like Fe. The intensity is given by

$$I_w = (1+\epsilon) \times \frac{N(\mathrm{Fe}^{+24}) N_e V}{4\pi(1\mathrm{AU})^2} \times \frac{8.63 \times 10^{-6}\, \Upsilon \exp(-E_0/k_B T_e)}{T_e^{1/2}} \qquad \text{photons cm}^{-2}\text{s}^{-1} \quad (1)$$

where $N(\mathrm{Fe}^{+24})$ is the number density of He-like Fe ions, E_0 the line's excitation energy, k_B Boltzmann's constant, and E_0 and Υ are respectively the excitation energy and the temperature-averaged collision strength of the transition.

The atomic data of Bely-Dubau et al. (1982) were used to calculate I_w; recent R-matrix collisional excitation data (?) are insignificantly different. Expressing $N(\mathrm{Fe}^{+24}) = N(\mathrm{Fe}^{+24})/N(\mathrm{Fe}) \times A_{\rm flare}(\mathrm{Fe})$, we took the ion fractions of Mazzotta et al. (1998) and a coronal Fe abundance relative to H, $A_{\rm cor} = 1.26 \times 10^{-4}$ (Feldman & Laming 2000) for A_{flare}. Lines x, y, and z (6.63–6.68 keV), are partly formed by collisional excitation from the He-like ion's ground state but with contributions from recombination of the H-like ion (at higher T_e) and (for line z) inner-shell ionization of the Li-like ion. Their intensities were

also from Bely-Dubau et al. (1982).

Satellite lines formed by dielectronic recombination (e.g. j) have intensities (Gabriel 1972; Bely-Dubau et al. 1982)

$$I_s = \frac{N(\mathrm{Fe}^{+24})N_e V}{4\pi(1\mathrm{AU})^2} \times \frac{2.07 \times 10^{-16}\, F_s}{T_e^{3/2}} \times \exp(-E_s/k_B T_e) \qquad \text{photons cm}^{-2}\text{s}^{-1} \qquad (2)$$

where F_s is given by

$$F_s = \frac{g_s\, A_r\, A_a}{A_a + \Sigma A_r}, \qquad (3)$$

g_s being the statistical weight of the satellite's lower level, A_r the radiative transition rate from the satellite's doubly excited upper level, A_a the corresponding auto-ionization rate, ΣA_r the sum of all possible radiative transition rates from the upper level, and E_s the satellite's transition energy. Values of I_s were calculated for j and other satellites using the atomic data of Bely-Dubau et al. (1979), Bely-Dubau et al. (1982), and Lemen et al. (1984).

The inner-shell $n = 2$ satellites (e.g. q) have intensities given by

$$I'_s = \frac{N(\mathrm{Fe}^{+23})N_e V}{4\pi(1\mathrm{AU})^2} \times \frac{8.63 \times 10^{-6}\, \Upsilon_s \exp(-E_s/k_B T_e)}{T_e^{1/2}} \qquad \text{photons cm}^{-2}\text{s}^{-1} \qquad (4)$$

where $N(\mathrm{Fe}^{+23})$ is the number density of Fe^{+23} ions ($= N(\mathrm{Fe}^{+23})/N(\mathrm{Fe}) \times A_{\mathrm{flare}}(\mathrm{Fe})$) and Υ_s is the temperature-averaged collision strength of the satellite line transition. There is hence a T_e-dependence through the ionization fraction $N(\mathrm{Fe}^{+23})/N(\mathrm{Fe}^{+24})$. Values of I'_s were calculated using data of Lemen et al. (1984) and ionization fractions of Mazzotta et al. (1998).

Similar expressions to these give the intensity ratios of satellites, dielectronic or inner-shell, emitted by lower Fe ionization stages (Fe XIX–Fe XXIII: 6.50–6.62 keV) but with ionization fractions $N(\mathrm{Fe}^{+18})$ to $N(\mathrm{Fe}^{+22})$. The intensity of the Fe XXIII line β was calculated as representative of these satellites.

The Fe fluorescence Kα lines (6.387, 6.400 keV) formed in or near the photosphere have intensity $I_{\mathrm{K}\alpha}$ given by (Bai 1979)

$$I_{\mathrm{K}\alpha} = \frac{\Gamma(h)\, f(h,\theta)}{1+\alpha(h,\theta)} \int_{I_K}^{\infty} I_c^{\mathrm{tot}}(E)\, dE. \tag{5}$$

Here, Γ is the Kα fluorescence efficiency (ratio of emitted Kα photons s^{-1} to $\frac{1}{2}\int_{I_K}^{\infty} I_c^{\mathrm{tot}} dE$ where I_c^{tot} is the the total continuum flux at Earth); $f(h,\theta)$ a factor expressing the dependence of $I_{\mathrm{K}\alpha}$ on θ, the heliocentric angle between the observer and flare and its height h above the photosphere; and α an albedo factor allowing for the amount of continuum radiation Compton-scattered by the photosphere. We may take I_c^{tot} to be the thermal bremsstrahlung spectrum,

$$I_c(E,T_e) = 1.03\times10^{-11} \times \frac{g_c \exp(-E/k_B T_e)}{E\, T_e^{1/2}} \times \frac{N_e N(\mathrm{H}) V}{4\pi(\mathrm{AU})^2} \tag{6}$$

where g_c is the free-free Gaunt factor, of order 1 (Mewe et al. 1985a). Both Γ and α are slowly decreasing functions of h. For typical flare heights $h = 10000 - 30000$ km and a photospheric Fe abundance ($A_{\mathrm{ph}}(\mathrm{Fe}) = N(\mathrm{Fe})/N(\mathrm{H}) = 3.2\times10^{-5}$: Grevesse & Sauval (1998)), $\Gamma \approx 0.015 \pm 20\%$, $\alpha \approx 0.06 \pm 0.02$, $f(h, \theta = 0) = 1.5 \pm 0.05$, and so for a typical flare at Sun center, the Fe Kα line intensity is

$$I_{\mathrm{K}\alpha} = 5.4\times10^{-5} \times \frac{N_e N(\mathrm{H}) V}{4\pi(1\mathrm{AU})^2} \times \frac{A_{\mathrm{ph}}(\mathrm{Fe})\, g_c\, E_1(I_K/k_B T_e)}{T_e^{1/2}} \tag{7}$$

where E_1 is the first logarithmic integral. This equation was used to calculate $I_{\mathrm{K}\alpha}$ with T_e assumed to be the temperature of the flare plasma, i.e. that used in Eqs. (1), (2), and (4). The Fe Kβ lines (7.05–7.10 keV) have an intensity of $\sim 0.13 \times I_{K\alpha}$.

Finally, the Fe XXVI Lyα doublet (6.947, 6.969 keV) contributes significantly to the Fe line feature at $T_e \gtrsim 30$ MK. Like Fe XXV line w, the lines are mainly collisionally excited, with small contributions made by cascades. High-n satellites, spectroscopically indistinguishable from the Lyα lines, contribute to the total intensity, up to 30% at $T_e = 20$ MK. Fe XXV satellites like those making up J (6.920 keV) have intensities given by expressions similar to Eq. (2).

Fig. 1 shows the contributions, as a function of T_e, of the individual lines mentioned above to the Fe-line feature. The 'total' emission in the Fe-line feature in this figure is given by the sum of all lines in the 5.8–7.5 keV range except the Fe Kα and Kβ lines from the Chianti atomic database and code (Dere et al. (1997): version 4.02). Fig. 1 shows that for $T_e \lesssim 70$ MK Fe XXV line w dominates, and for $T_e \gtrsim 85$ MK the Fe XXVI Lyα lines are the largest contributor. The maximum of the total curve is at $T_e \sim 75$ MK, far higher than the range (approximately 20–30 MK) of the thermal component of most solar flares. Fe XXIV dielectronic satellites exceed the intensity of line w for $T_e \lesssim 15$ MK. For T_e as high as 30 MK, the total contribution of all dielectronic satellites is still a significant fraction of I_w. Satellite q, the most intense of the relatively few inner-shell satellites, is comparable to j. Satellite emission from lower stages adds only a small amount of emission at $T_e \lesssim 20$ MK. Satellite J near the Fe XXVI Lyα lines is a significant fraction of the Fe XXVI lines for $T_e \lesssim 30$ MK, but at these temperatures, Fe XXV line w dominates.

For the coronal (Feldman & Laming 2000) abundances assumed here, the photospheric Fe Kα lines make only a small ($\lesssim 4\%$) contribution to the total in this temperature range, but the contribution increases with T_e because of the increase of $\int_{I_K}^{\infty} I_c^{\mathrm{tot}}(E)dE$. Moreover,

for a flare plasma with photospheric Fe abundance (as with the impulsive *Skylab* flare cited by Feldman & Laming (2000)), i.e. one with $A_{\rm flare}$(Fe) that is ~ 0.25 times less than the coronal value assumed above, all the contribution functions in Fig. 1 will decrease by a factor 4 compared with the Fe Kα curve; the Fe Kα lines will then be as much as $\sim 15\%$ of the total at $T_e = 100$ MK.

The Fe/Ni-line feature (7.5–9:2 keV) includes Fe XXV $1s^2 - 1snp$ and Fe XXVI $1s - np$ ($n \geq 3$) lines which are, like the $n = 2$ lines, collisionally excited and so have intensities given by Eq. (1) with Υ appropriate for each transition. There is no appreciable satellite emission on the low-energy side of each line (de-excitation of e.g. $1s2p3p$ states is mostly to $1s3p$ rather than to $1s2p$) and Fe XXV intercombination and forbidden lines do not occur since states like $1s3p\,^3P$ or $1s3s\,^3S$ de-excite to $1s^22s\,^3S$ or $1s^22p\,^3P$ rather than to $1s^2\,^1S_0$. The Fe/Ni feature also includes Ni XXVII $1s^2 - nl$ ($n = 2, 3$; $l = s, p$: 7.73–9.177 keV), analogous to Fe XXV lines, and the Ni XXVIII Lyα lines (8.096, 8.067 keV), analogous to Fe XXVI lines. They are less intense than the equivalent Fe lines because the Ni abundance (coronal or photospheric) is a factor 20 smaller than that of Fe, and also because they have higher excitation temperatures.

Fig. 2 shows the contributions of individual lines to the Fe/Ni-line feature as a function of T_e. In this figure, the 'total' emission is the sum of all lines in the range 7.5–9.2 keV from Chianti. At maximum (at $T_e \sim 90$ MK), the Fe/Ni-line feature is only about 10% that of the Fe-line feature. Fig. 2 shows that the major part of the Fe/Ni-line feature is made up of the Fe XXV $1s^2 - 1s3p$ ($T_e \lesssim 80$ MK) and the Fe XXVI Lyβ lines. The Ni XXVII line w is only 15% of the intensity of the Fe XXV line at $T_e \sim 20$ MK. The contribution of all Ni XXVII, Ni XXVIII lines and their satellites is never more than about 25% of the total, so the Fe/Ni-line feature is in fact mostly made up of Fe lines.

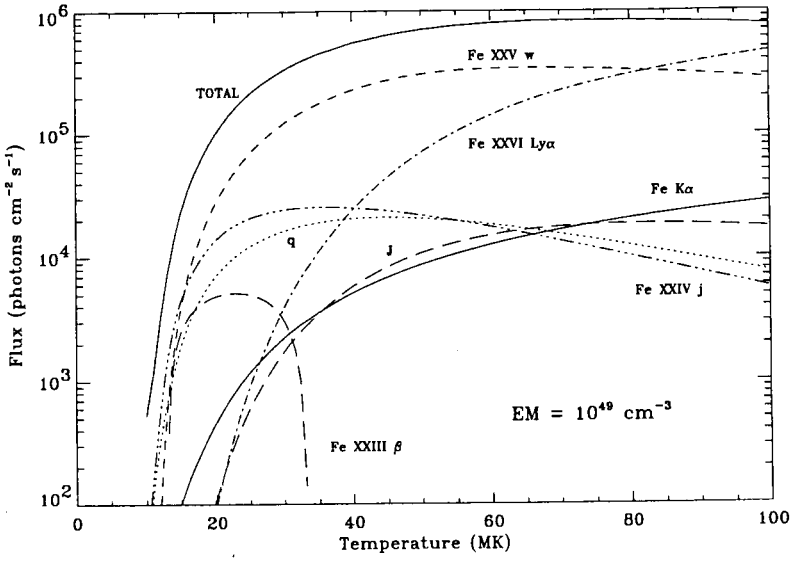

Fig. 1.— Contribution of principal emission lines (labelled) making up the 7 keV Fe-line feature. The curve labelled "Total" is the total emission in the line feature between 5.8 and 7.5 keV as estimated from Chianti. A coronal (Feldman & Laming 2000) abundances of Fe was assumed for all lines except the Fe Kα lines for which a photospheric Fe abundance (Grevesse & Sauval 1998) was assumed.

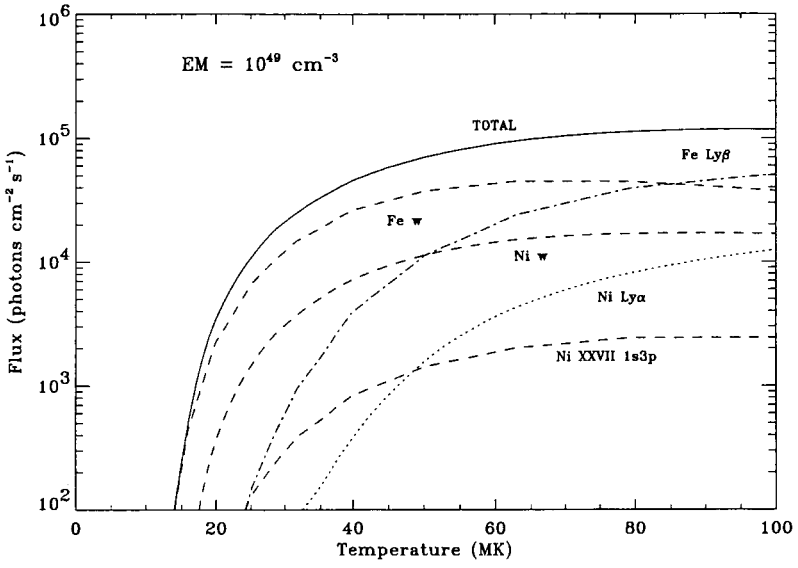

Fig. 2.— Contribution of principal emission lines (labelled) making up the 8 keV Fe/Ni-line feature. The curve labelled "Total" is the total emission in the line feature between 7.5 and 9.2 keV as estimated from Chianti.

2.3. Centroid and Peak Energies of the Fe-Line Feature

The Fe-line and Fe/Ni-line features as viewed by a broad-band spectrometer like *RHESSI* are thus made up of many individual lines each having its own temperature dependence. Their contribution to the total emission of either the Fe-line or Fe/Ni-line feature will therefore change as the temperature of a solar flare plasma changes in both space and time. This results in changes to the energies of the Fe-line and Fe/Ni-line features, as defined by the peak (E_p) or centroid ($E_c = \int E\, I(E) dE / \int I(E) dE$, $I(E) =$ spectral intensity at energy E, integrals over the range of each line feature). Changes in E_p and E_c, if large enough, therefore provide a possible useful temperature diagnostic. We assume that the continuum contribution to the spectrum has been subtracted. As the Fe/Ni-line feature is relatively weak, we examine only the case of the Fe-line feature.

For the Fe XXV lines and their satellites, increasing T_e results in decreasing the intensities of satellites, both dielectronic and inner-shell, relative to line w. For $T_e < 30$ MK, when Fe XXVI line emission is insignificant, E_p and E_c should be less than the energy of line w (6.696 keV), but increasing slightly with T_e as the dielectronic and inner-shell satellites decrease relative to line w. For particularly hot ($T_e \gtrsim 30$ MK) flares, for which there is significant Fe XXVI line (6.947, 6.969 keV) emission, E_p or E_c is expected to shift to energies greater than line w. Unless the flare abundance of Fe is much less than the coronal value, the Fe Kα lines will always be too weak to produce any counter-effect through their increase during the flare rise.

Synthetic spectra from the Chianti code in the 4–10 keV range were used to find changes in E_p and E_c with T_e. The spectra, which are given in terms of wavelength, were first synthesized without continuum contributions at 1 MK intervals, and transformed to an energy scale. They were then convolved with a gaussian curve having a FWHM of 0.8 keV to match the spectral resolution of detector 4 of *RHESSI*. The values of E_p and E_c (different

by $\lesssim 0.01$ keV) derived are plotted against T_e in Fig. 3. The Fe-line feature is too weak to be observable when $T_e \lesssim 12$ MK. At higher T_e, there is a slow rise in E_p and E_c from 6.63 to 6.70 keV over the range $T_e = 15 - 45$ MK as the Fe XXIV satellites decrease relative to line w. For $T_e \gtrsim 45$ MK, the rise with T_e is slightly accelerated as the Fe XXVI Lyα lines become more significant. The rise of E_p and E_c over the temperature range of most flares, though modest, is barely measurable with *RHESSI* – although the energy resolution at 7 keV is 0.8 keV, gaussian-fitting techniques enable the peak and centroid energies to be defined to ~ 0.01 keV for strong events. However, an unexpected change of gain with count rate has made this goal unachievable at present.

A check on the validity of Fig. 3 for $T_e \lesssim 35$ MK is provided by high-resolution flare observations of the Fe-line feature made with the *SMM* Bent Crystal Spectrometer (energy range 6.4–7.0 keV) and the *Yohkoh* Bragg Crystal Spectrometer (6.6–7.1 keV). Two very large flares (1980 July 1, seen by *SMM*, and 1991 December 16 seen by *Yohkoh*) were selected for which Fe XXVI line emission was detected. The *SMM* spectrometer energy range includes satellite lines from lower Fe ionization stages. Its high resolving power ($\Delta E/E \sim 4000$) enabled accurate I_j/I_w line ratios to be obtained, leading to temperature uncertainties $\Delta T_e \sim \pm 0.5$ MK. The spectra from the *Yohkoh* instrument, although having lower resolution ($E/\Delta E \sim 1000$), can nevertheless be analyzed with spectral fitting routines to give $\Delta T_e = \pm 1$ MK uncertainties. Several spectra over the course of each flare were convolved with a gaussian filter having FWHM = 0.8 keV, and E_c and E_p were derived. The values of these energies have uncertainties of about 0.02 keV, greater at lower T_e when the line emission is weaker relative to an instrumental background present for both spectrometers. Fig. 4 is a plot of observed values of E_c and T_e compared with the curve derived from Chianti spectra. The agreement between the curves and all but two of the observed points is better than ± 0.03 keV, adequate to show the predicted increase of E_c with T_e over this temperature range. This comparison confirms the validity of the Chianti

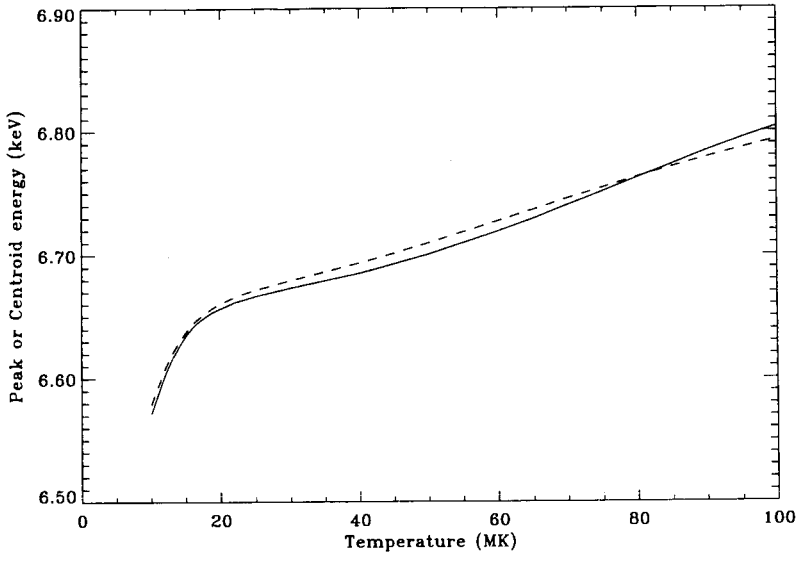

Fig. 3.— Peak (full line) and centroid (dashed line) energies as a function of T_e of the Fe-line feature observed by a spectrometer like *RHESSI*, having FWHM= 0.8 keV resolution.

synthetic spectra in this range, and the diagnostic potential of E_p or E_c of flare temperature.

2.4. Intensity Ratio of Fe-line and Fe/Ni-line Features

The differing T_e sensitivity of the Fe-line and Fe/Ni-line features (Figs 1 and 2) means that the ratio of the features offers another method for determining T_e in addition to the peak or centroid energies of the Fe line. The intensity ratio, derived from Chianti, is shown in Fig. 5. For $T_e < 20$ MK, the Fe/Ni-line feature is too weak to be observed with *RHESSI*. The intensity ratio decreases by a factor of 2 from 20–30 MK, but at higher temperatures decreases much more slowly. This intensity ratio as a temperature diagnostic is therefore of limited use.

3. Line and Continuum Emission

3.1. Synthetic 4–10 keV Spectra

As indicated in §1, the Fe-line and Fe/Ni-line features are observed as emission excesses above a thermal continuum which decreases with T_e and photon energy E. Most of this continuum is bremsstrahlung emission, and approximately 90% of this is hydrogen bremsstrahlung. For $T_e \lesssim 20$ MK, free-bound emission contributes significantly to the 4–10 keV energy range, but is progressively less important for higher T_e (Culhane 1969; Mewe et al. 1985a). Much of the free-bound emission is from higher-Z elements like Fe and Ca. Two-photon continuum emission (from the radiative decay of meta-stable atomic states) is always negligible. The thermal continuum from the Chianti code is within 1% of the detailed calculations of Culhane (1969) and the approximations of Mewe et al. (1985a), so we use the Chianti calculations throughout this section.

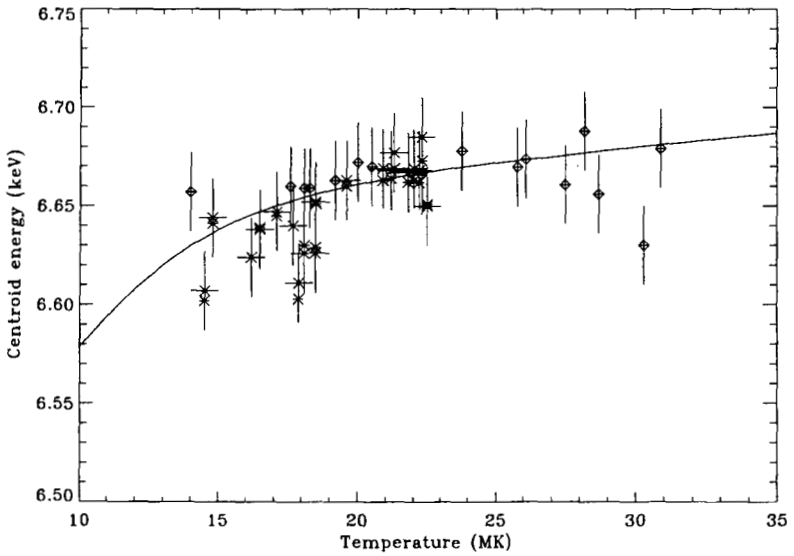

Fig. 4.— Centroid energy of the Fe line feature, observed with a spectrometer like *RHESSI* having a resolution with FWHM 0.8 keV, compared with observed points from the *SMM* Bent Crystal Spectrometer (stars) and the *Yohkoh* Bragg Crystal Spectrometer (diamonds) for large flares on 1980 July 1 and 1991 December 16 respectively.

Fig. 6 shows the synthetic spectra from Chianti in the 4–10 keV range for $8 < T_e < 33$ MK in 1 MK intervals. The original line and continuum spectrum for each temperature has been transformed to an energy (keV) scale and photon units per keV. Coronal element abundances (Feldman & Laming 2000) and the ion fractions of Mazzotta et al. (1998) were used. The spectra were convolved with a 0.8 keV FWHM gaussian, matching the *RHESSI* spectral resolution. These synthetic spectra show the progressive increase in the Fe-line and Fe/Ni-line features above the continuum with increasing T_e. The Fe-line feature only becomes visible above the continuum at $T_e \gtrsim 112$ MK. This is in agreement with Fig. 1 and *SMM* and *Yohkoh* BCS observations (Fig. 4). The *SMM* and *Yohkoh* observations confirm that the Fe^{+23}–Fe^{+25} ionization fractions in coronal equilibrium are more accurately given by Mazzotta et al. (1998) and Arnaud & Raymond (1992), which are based on improved ionization and recombination data, than the earlier Arnaud & Rothenflug (1985) work used extensively until the early 1990s, which indicated a significant Fe^{+24} fraction at $T_e \sim 10$ MK. It should be noted that routines calculating X-ray emission and temperatures in the SolarSoft package (e.g. using SPEX or from *GOES* channel ratios) are still based on the Arnaud & Rothenflug (1985) ionization fractions and so caution should be used in results derived from them at low temperatures.

3.2. Centroid and Peak Energies of Fe-line feature with Continuum

The centroid and peak energies of the Fe-line and Fe/Ni-line features in §2.3 are given on the assumption that the continuum can be accurately subtracted in observed spectra. Here we repeat the analysis with the continuum, again using the Chianti code. Fig. 7 shows these energies plotted against T_e. The variation, while similar to that shown in Fig. 3 for $T_e \gtrsim 25$ MK, is different for lower temperatures as the continuum is then so steeply declining with T_e that the centroid and peak energies, when defined with a gaussian filter of

0.8 keV FWHM, are significantly influenced by the continuum which is much more intense on the lower-energy side of the Fe line feature than on the higher-energy side. This explains the steep fall-off of centroid and more particularly the peak energy of the Fe-line feature towards lower T_e. As can be seen from Fig. 6, a maximum in the energy range 5.8–7.5 keV can only be defined for $T_e > 13$ MK.

3.3. Abundance of Fe in Flare Plasmas

The observation of the Fe-line feature and neighboring continuum, which is mostly hydrogen bremsstrahlung during flares, offers a means of determining the iron abundance $A_{\rm Fe}$ during flares. The thermal plasma during flares is located in the coronal loop structures typically 10^4 km above the photosphere. On a chromospheric evaporation picture, this plasma is formed from the chromosphere and so should reflect the chromospheric composition. Most analyses of flare X-ray and ultraviolet spectra (e.g. Fludra et al. (1999); ?) show that elements with a variety of first ionization potentials (FIPs) are in ratios that are characteristic of the corona rather than the photosphere, i.e. with low-FIP (FIP $\lesssim$ 10 eV) elements enhanced by a factor 3 or 4 but with high-FIP elements approximately the same or depleted by up to a factor of 2 compared with photospheric abundances. However, Feldman & Laming (2000) cite the case of a fast flare event observed with the ultraviolet spectrometer on *Skylab* which showed photospheric abundances. In addition, observations from *SMM* (Sylwester, Lemen, & Mewe 1984) indicate significant flare-to-flare variations. It is possible, then, that flare abundances are related to flare duration or some property that is determined by the nature of the chromospheric evaporation or other process that gives rise to the thermal plasma contained in coronal loops in flares. Since both Fe and Ni are low-FIP elements, *RHESSI* observations of the Fe-line feature with neighboring continuum which allow the flare Fe abundance to be determined will give a valuable new

diagnostic tool.

A measure of the Fe-line feature's intensity with respect to the continuum is provided by the equivalent width, measured in keV, which can be determined from *RHESSI* spectra. Chianti spectra convolved with a gaussian of FWHM 0.8 keV to simulate the spectral resolution of *RHESSI* (Fig. 6, calculated for a coronal Fe abundance) permit theoretical equivalent widths to be determined as a function of T_e. *RHESSI* observations of the flare thermal component may be analyzed to give T_e with fitting programs comparing the model and measured continuum spectra. Comparison of the equivalent width at an observed T_e with that calculated from this figure should give A(Fe) in terms of the coronal abundance. Alternatively, if a value of A(Fe) can be assumed then the equivalent width gives an estimate of the plasma temperatures.

4. Ionization Conditions in Flares

Eqs (1), (32), and (4) assume a steady-state ionization equilibrium in the flare plasma. However, since temperature changes, particularly in the flare rise phase, are sometimes very rapid, the validity of this assumption might be questioned. Thus, during the rise, the plasma is in an ionizing state, i.e. there are greater proportions of lower ionization stages than the instantaneous value of T_e would indicate. During the decay, the plasma is cooling and in a recombining state, i.e. there are greater proportions of higher ionization stages. The time-dependent fraction of a particular ionization stage i ($N_i/N_{\rm Fe}$ in the case of Fe ions) is then governed by rate coefficients of ionization (Q) and recombination (α) rate coefficients from and to this stage:

$$\frac{1}{N_e}\frac{dN_i}{dT_e}\frac{dT_e}{dt} = Q_{i-1}N_{i-1} - N_i(Q_i + \alpha_i) + \alpha_{i+1}N_{i+1}, \tag{8}$$

with the observed temperature changes defined by dT_e/dt. Time-dependent calculations solving for N_i have been done for flare plasmas by Phillips et al. (1974) and Mewe et al. (1985b). They show that unless T_e changes are very rapid $dT_e/dt \gtrsim 5$ K s^{-1}, ionization equilibrium is likely to be a good approximation unless $N_e \lesssim 10^{10}$ cm^{-3}. Mewe et al. (1985b) using chromospheric evaporation models show that time-dependent effects are significant for the impulsive stage, though the exact details depend on the dynamic effects included in the model.

This is illustrated for the case of the 1991 December 16 flare observed by *Yohkoh*, which was large but relatively short-lived and therefore likely to show possible time-dependent effects. Fig. 9 shows three curves, the BCS light-curve in the Fe XXV channel, T_e, and values of $(dT_e/dt)/T_e$ derived as a function of time from satellite-to-line w intensity ratios. Values of $(dT_e/dt)/T_e$ when T_e is rising ($dT_e/dt > 0$) are compared with inverse ionization times $1/\tau_i$ where

$$\tau_i = \frac{1}{Q_i N_e} \tag{9}$$

where Q_i is the rate coefficient (cm^3 s^{-1}) for ionization of Fe^{+23} to Fe^{+24} ions and N_e is assumed to be 10^{10} cm^{-3}. Similarly, when T_e is falling, values of $(dT_e/dt)/T_e$ (< 0) are compared with inverse recombination times $1/\tau_r$ where

$$\tau_r = \frac{1}{\alpha_i N_e} \tag{10}$$

where α_i is the rate coefficient for recombination of Fe^{+25} to Fe^{+24} ions and again $N_e = 10^{10}$ cm^{-3}. Fig. 9 shows that the time changes, though relatively rapid, are much less than the Fe^{+24} ionization and recombination times for $N_e = 10^{10}$ cm^{-3}. Larger densities (as are indicated by line ratios, e.g. Doschek et al. (1981), Phillips et al. (1996), immediately

after the impulsive stage) give correspondingly shorter ionization and recombination times.

An isothermal plasma is implicit in Eqs (1), (2), and (4) and in the discussion so far, but more realistically the plasma has a nonthermal temperature structure, describable by a differential emission measure DEM = $N_e^2 dV/dT_e$). Procedures for deriving the flare DEM from crystal spectrometer data are outlined by Fludra et al. (1999) but for flare spectra observed by *RHESSI* one must resort to DEMs from flare loop models (McTiernan et al. 1999) or analytical approximations with parameters from the continuum slope (?). Imaging spectroscopy also provides another tool to separate plasma with different temperatures and allow the DEM to be determined spectroscopically.

5. Summary and Applications to Non-solar sources

The 4–10 keV spectral region of solar flares includes atomic lines from highly stripped ions of elements such as Ca, Fe, and Ni, having the largest excitation energies of any atomic transitions. These lines potentially provide diagnostic information about the hottest plasma produced during flares. Table 1 gives details of the principal lines over the 4–10 keV range. Two line groups, centered on $\sim$ 7 keV and $\sim$ 8 keV, are made up largely of Fe lines but with some Ni line emission at $\sim$ 8 keV. With a broad-band instrument (energy resolution $\sim$ 0.8 keV) such as *RHESSI* or *NEAR*-PIN, these groups of lines form line features called here the Fe-line and Fe/Ni-line features, defined by excess emission over the continuum in the ranges 5.8–7.5 keV and 7.5–9.2 keV respectively. An instrument like *RHESSI* could use the peak or centroid energies (E_p or E_c) of the more intense Fe-line feature to determine T_e for comparison with that found from the continuum, assumed thermal in origin. Also, the thermal and nonthermal components of the measured continuum spectrum can be more cleanly separated if temperature and emission measure can be independently determined from the two line complexes. For $15 < T_e < 35$ MK (typical of *RHESSI* flares), E_c changes

from 6.61 to 6.68 keV (continuum subtracted) which is barely measurable with *RHESSI*. The fluorescence-formed Fe Kα lines make only a very small contribution to the Fe-line feature at these temperatures but this contribution increases with T_e. In principle, the intensity ratio of the Fe-line and Fe/Ni-line features is temperature-sensitive but this ratio is only useful if the Fe/Ni -line feature is easily measurable and if $T_e < 30$ MK, leaving only a limited T_e range. The equivalent width of the Fe-line feature gives the best temperature diagnostic. There is a strong dependence with T_e from 15 MK to 35 MK. However, the equivalent width also depends on the abundance of Fe in the flaring plasma; this is thought to vary from flare to flare, possibly also during the course of each flare. The calculated equivalent widths given here assume coronal abundances, where the abundance of low-FIP elements are taken to be four times photospheric. If T_e can be determined from the flare continuum (nonthermal contribution in the 4–10 keV range assumed to be negligible), the equivalent width of the Fe line can then be used to investigate possible Fe abundance variations. Finally, we show that in spite of rapidly varying T_e during flares, ionization equilibrium can be assumed for Fe ions in most circumstances.

The results here should be applicable to non-solar X-ray-emitting plasmas such as those formed in stellar flares, the hot gas in some galaxies and clusters of galaxies, and older supernova remnants, or for any source for which photo-ionization contributes little to the ionization equilibrium. They would not be applicable to X-ray sources such as accretion-powered systems (X-ray binaries, some active galactic nuclei) where there is a strong photo-ionizing continuum present. Spectrometers aboard the *Exosat*, *Ginga*, and *Tenma* spacecraft had spectral resolutions of about 1 keV at the energy of the Fe line, so the results given here could be applied to their spectra. Higher-resolution spectrometers now operating on the *Chandra* and XMM-Newton spacecraft ($\sim$ 200 eV at the Fe line feature's energy) are partially able to resolve the satellite structure of the Fe lines and so could possibly obtain better temperature and abundance information than for broad-band

instruments.

This research was made possible through a National Research Council Research Associateship award at NASA Goddard Space Flight Center. Cristina Chifor, Brian R. Dennis, Enrico Landi, and Hugh Hudson are sincerely thanked for their contributions to this paper.

Table 1. Solar Flare Lines in the 3.8–10 keV Range

Ion	Energy (keV)[c]	λ (Å)	Transition	Line label[d]	Rel. int. (20 MK)[a]	Rel. int. (100 MK)[a]
Ca XIX	3.859	3.2108	$1s^2 - 1s2s$	z	12.4	
Ca XIX	3.881	3.1925	$1s^2\,{}^1S_0 - 1s2p\,{}^3P_1$	y	6.7	3.8
Ca XIX	3.885	3.1889	$1s^2\,{}^1S_0 - 1s2p\,{}^3P_2$	x	6.3	3.7
Ca XIX	3.900	3.1769	$1s^2\,{}^1S_0 - 1s2p\,{}^1P_1$	w	34.5	7.8
Ar XVIII	3.933	3.1506	$1s - 3p$	Lyβ	2.1	4.4
Ca XIX	4.067	3.049	$1s2p\,{}^1P_1 - 2p^2\,{}^1D_2$	J		
Ca XX	4.105,4.097	3.0185,3.0239	$1s\,{}^2S_{1/2} - 2p\,{}^2P_{3/2,1/2}$	Lyα	3.5,2.3	20.0,11.6
Ar XVIII	4.147	2.9875	$1s - 4p$	Lyγ		3.5
Ca XIX	4.579	2.706	$1s^2 - 1s3p$	3.4		3.1
Ca XIX	4.815	2.573	$1s^2 - 1s4p$			2.6
Ca XX	4.860	2.5494	$1s - 3p$	Lyβ	0.8	4.3
Ca XX	5.125	2.4174	$1s - 4p$	Lyγ		2.8
Ca XX	5.248	2.3609	$1s - 5p$	Lyδ		
Fe II, III	6.400,6.387	1.9360,1.9400	$[1s\,{}^2S_{1/2}] - [2p\,{}^2P_{3/2}]^b$	Kα_1,Kα_2		
Fe XX	6.501	1.906	$1s^22s^22p^3 - 1s2s^22p^4$	Sats.[e]		
Fe XXI	6.548	1.892	$1s^22s^22p^2 - 1s2s^22p^3$	Sats.[e]	1.8	1.5
Fe XXII	6.573	1.885	$1s^22s^22p - 1s2s^22p^2$	Sats.[e]		
Fe XXIII	6.624	1.8704	$1s^22s^2 - 1s2s^22p$	Sats.[e]		
Fe XXV	6.632	1.8689	$1s^2\,{}^1S_0 - 1s2s\,{}^3S_1$	z	4.8	16.1
Fe XXIV	6.638	1.8666	$1s^22p\,{}^2P_{1/2} - 1s2p^2\,{}^2D_{5/2}$	j		
Fe XXIV	6.648	1.8638	$1s^22p\,{}^2P_{1/2} - 1s2p^2\,{}^2D_{3/2}$	k		
Fe XXIV	6.665	1.8617	$1s^22s\,{}^2S_{1/2} - 1s2s2p\,{}^2P_{3/2}$	q		
Fe XXV	6.663	1.8602	$1s^2\,{}^1S_0 - 1s2p\,{}^3P_1$	y	6.1	20.6
Fe XXIV	6.670	1.8575	$1s^22s\,{}^2S_{1/2} - 1s2s2p\,{}^2P_{1/2}$	t		
Fe XXV	6.678	1.8561	$1s^2\,{}^1S_0 - 1s2p\,{}^3P_2$	x	3.4	10.9
Fe XXV	6.696	1.8509	$1s^2\,{}^1S_0 - 1s2p\,{}^1P_1$	w	12.0	116.2
Fe XXV	6.920	1.7917	$1s2p\,{}^1P_1 - 2p^2\,{}^1D_2$	J	0.1	12.0
Fe XXV	6.919	1.7921	$1s2p\,{}^3P_2 - 2p^2\,{}^3P_2$			
Fe XXV	6.938	1.7870	$1s2s\,{}^3P_2 - 2p^2\,{}^1D_2$	Sat.		
Fe XXV	6.942	1.7861	$1s2s\,{}^1S_0 - 2s2p\,{}^1P_1$	Sat.		
Fe XXVI	6.947	1.7834	$1s\,{}^2S_{1/2} - 2p\,{}^2P_{1/2}$	Lyα_2	0.1	38.9
Fe XXV	6.951	1.7824	$1s2p - 2p^2$	Sat.		

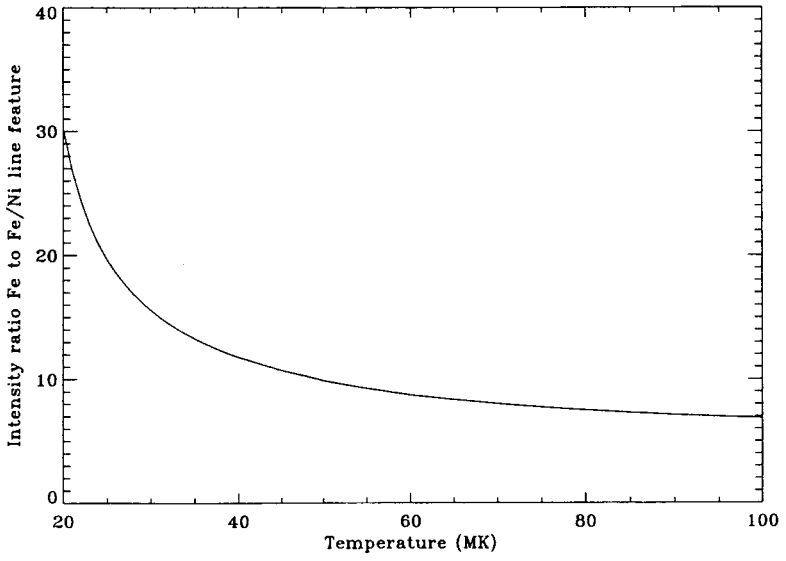

Fig. 5.— Intensity ratio of the Fe-line and Fe/Ni-line features as a function of T_e.

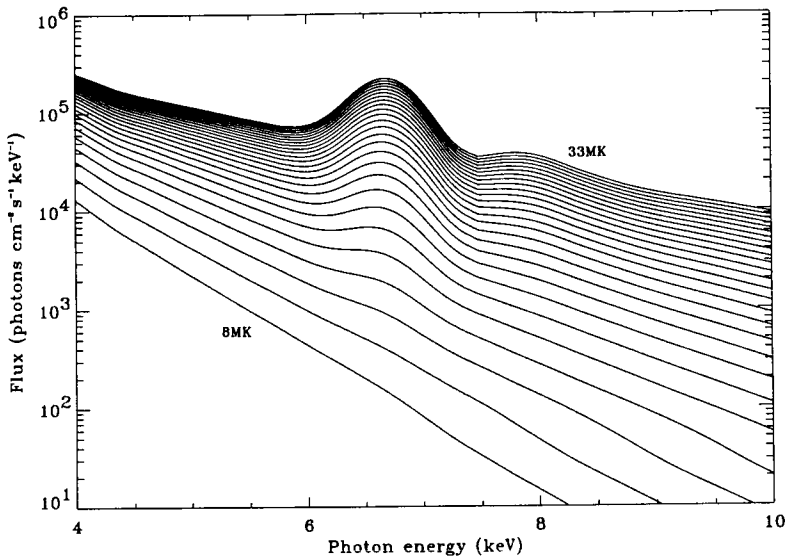

Fig. 6.— Synthetic spectra between 4 and 10 keV from the Chianti code, with coronal abundances of Fe and Ni, smoothed with a gaussian filter having FWHM = 0.8 keV. Spectra are given in 1 MK intervals from 8 MK to 33 MK and for an emission measure $\int_V N_e^2 dV = 10^{49}$ cm^{-3}.

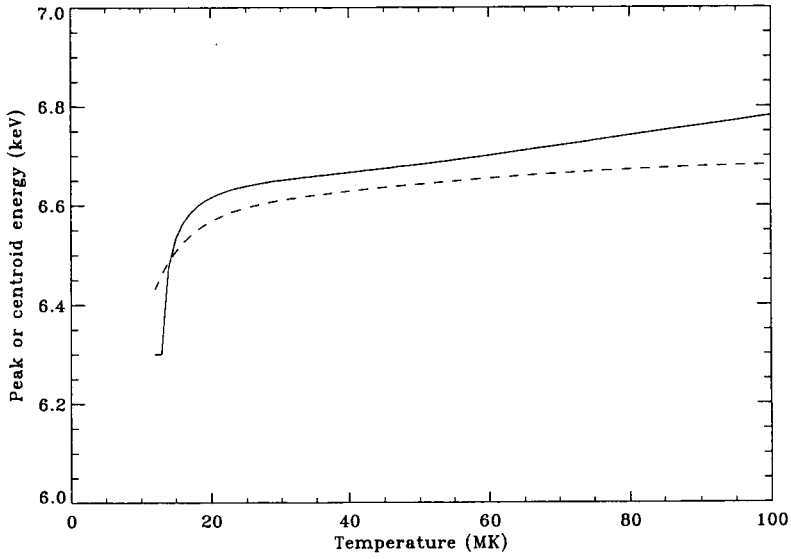

Fig. 7.— Peak (full line) and centroid (dashed line) energies of the Fe-line feature with continuum included plotted as a function of T_e. The energies have been derived assuming a gaussian filter with FWHM = 0.8 keV.

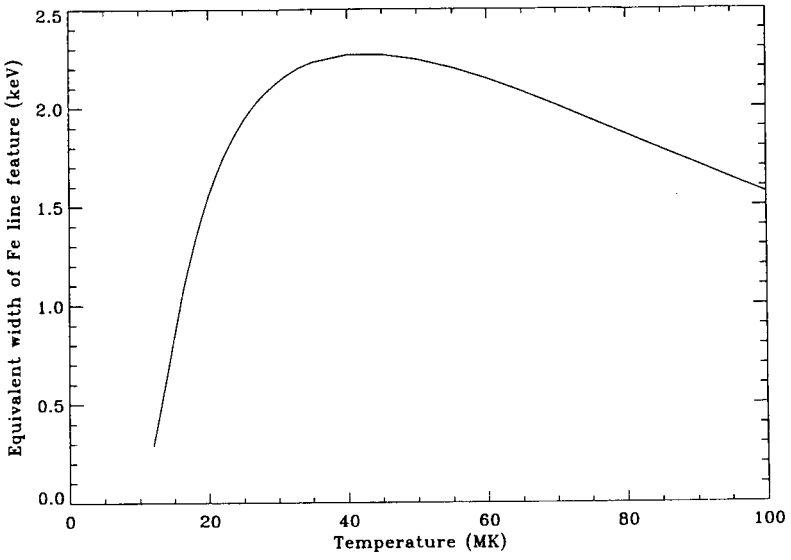

Fig. 8.— The equivalent width of the Fe-line feature (keV) as a function of T_e, calculated from the Chianti code with the coronal abundances of Feldman & Laming (2000).

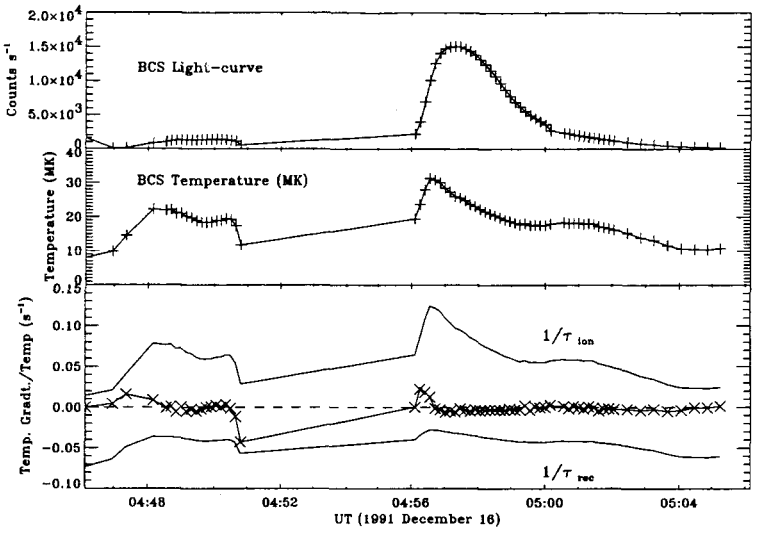

Fig. 9.— Light-curve (*top panel*) and T_e (*middle panel*) from *Yohkoh* BCS Fe XXV spectra, together with values of $(dT_e/dt)/T_e$ (*bottom panel*) derived from the temperature variations, for the large flare on 1991 December 16. Positive values of $(dT_e/dt)/T_e$, i.e. during temperature rise phases, are compared with inverse ionization times $1/\tau_{\rm ion}$ for $N_e = 10^{10}$ cm^{-3}, negative values with inverse recombination times $1/\tau_{\rm rec}$.

Table 1—Continued

Ion	Energy (keV)[c]	λ (Å)	Transition	Line label[d]	Rel. int. (20 MK)[a]	Rel. int. (100 MK)[a]
Fe XXVI	6.969	1.7780	$1s\,^2S_{1/2} - 2p\,^2P_{3/2}$	Lyα_1	0.1	72.6
Fe II, III	7.104,7.052	1.744,1.757	$[1s] - [3p]^b$	Kβ		
Ni XXVI	7.510	1.650	$1s^2\,2p\,^2P - 1s2p^2\,^2D$	Sats.		
Ni XXVII	7.726	1.6036	$1s^2\,^1S_0 - 1s2s\,^3S_1$	z		1.6
Ni XXVII	7.760	1.5966	$1s^2\,^1S_0 - 1s2p\,^3P_1$	y	0.2	2.0
Ni XXVII	7.781	1.5923	$1s^2\,^1S_0 - 1s2p\,^3P_2$	x		
Ni XXVII	7.800	1.5885	$1s^2\,^1S_0 - 1s2p\,^1P_1$	w	0.2	6.0
Fe XXV	7.876	1.5732	$1s^2\,^1S_0 - 1s3p\,^1P_1$		0.7	12.3
Ni XXVIII	8.096,8.067	1.5303,1.5358	$1s\,^2S_{1/2} - 2p\,^2P_{3/2,1/2}$	Lyα		2.5,1.7
Fe XXVI	8.247,8.241	1.5024,1.5035	$1s\,^2S_{1/2} - 3p\,^2P_{3/2,1/2}$	Lyβ		9.0
Fe XXV	8.290	1.4945	$1s^2\,^1S_0 - 1s4p\,^1P_1$		0.2	4.4
Fe XXV	8.480	1.461	$1s^2\,^1S_0 - 1s5p\,^1P_1$		0.1	2.3
Fe XXV	8.586	1.443	$1s^2\,^1S_0 - 1s6p\,^1P_1$			
Fe XXVI	8.694	1.4251	$1s\,^2S_{1/2} - 3p\,^2P_{3/2,1/2}$	Lyγ		3.4
Fe XXVI	8.901	1.392	$1s - 5p$	Lyδ		1.9
Ni XXVII	9.177	1.3501	$1s^2\,^1S_0 - 1s3p\,^1P_1$			1.2
Ni XXVIII	9.582,9.568	1.293,1.296	$1s\,^2S_{1/2} - 3p\,^2P_{3/2,1/2}$	Lyβ		0.8
Ni XXVII	9.657	1.283	$1s^2\,^1S_0 - 1s4p\,^1P_1$			0.7
Ni XXVII	9.880	1.254	$1s^2\,^1S_0 - 1s5p\,^1P_1$			0.6
Ni XXVII	10.008	1.238	$1s^2\,^1S_0 - 1s6p\,^1P_1$			
Ni XXVIII	10.098	1.227	$1s - 4p$	Lyγ		0.6
Ni XXVIII	10.342	1.198	$1s - 5p$	Lyδ		0.5

[a]From Chianti calculated spectra.

[b]Square brackets indicate hole transitions.

[c]Line energies (wavelengths) from Hata & Grant (1982), Sevier (1979), Ermolaev & Jones (1973), Erickson (1977), Doschek et al. (1979)

[d]Line labels are from Gabriel (1972) for He-like Fe and Ni. "Sat." or "sats." refers to dielectronic satellite(s); when several satellites occur, a mean energy energy is given.

[e]Details of these satellites are given by Phillips et al. (1983) and Lemen et al. (1984).

REFERENCES

Acton, L. W., et al. 1980, Sol. Phys., 65, 53

Arnaud, M., & Raymond, J. 1992, ApJ, 398, 394

Arnaud, M., & Rothenflug, R. 1985, A&AS, 60, 425

Bai, T. 1979, Sol. Phys., 62, 113

Bambynek, W., Crasemann, B., Fink, R. W., Freund, H.-U., Mark, H., Swift, C. D., Price, R. E., & Rao, P. V. 1972, Rev. Mod. Phys., 44, 716

Bely-Dubau, F., Dubau, J., Faucher, P., & Gabriel, A. H. 1982, MNRAS, 198, 239

Bely-Dubau, F., Gabriel, A. H., & Volonté, S. 1979, MNRAS, 189, 801

Bitter, M., et al. 1979, Phys. Rev. Letts, 43, 129

Bitter, M., et al. 1991, Phys. Rev. A44, 1796

Bombarda, F., et al. 1988, Phys. Rev. A37, 504

Culhane, J. L. 1969, MNRAS, 144, 375

Culhane, J. L., et al. 1991, Sol. Phys., 136, 89

Dere, K. P., Landi, E., Mason, H. E., Monsignori Fossi, B. C., & Young, P. R. 1997, A&AS, 125, 149

Doschek, G. A., Feldman, U., Kreplin, R. W., & Cohen, L. 1980, ApJ, 239, 725

Doschek, G. A., Feldman, U., Landecker, P. B., & McKenzie, D. L. 1981, ApJ, 245, 315

Doschek, G. A., Kreplin, R. W., & Feldman, U. 1979, ApJL, 233, L157

Doschek, G. A., Meekins, J. F., Kreplin, R. W., Chubb, T. A., & Friedman, H. 1971, ApJ, 170, 573

Dubau, J., Gabriel, A. H., Loulergue, M., Steenman-Clark, L., & Volonté, S. 1981, MNRAS, 195, 705

Emslie, A.G., Phillips, K. J. H., & Dennis, B.R., 1986. Sol. Phys., 103, 89

Erickson, G. W. 1977, J. Phys. Chem. Ref. Data, 6, 831

Ermolaev, A. M., & Jones, M. 1973, J. Phys. B, 6, 1

Feldman, U., & Laming, M. 2000, Phys. Scripta, 61, 222

Fludra, A., & Schmelz, J. T. 1999, A&A, 348, 286

Gabriel, A. H. 1972, MNRAS, 160, 99

Grevesse, N., & Sauval, A. J. 1998, Space Sci. Rev., 85, 161

Hata, J., & Grant, I. P. 1982, MNRAS, 198, 1081

Lemen, J. R., Phillips, K. J. H., Cowan, R. D., Hata, J., & Grant, I. P. 1984, A&A, 135, 313

Lin, R. P. et al. 2002, Sol. Phys., 210, 3

Masuda, S., Kosugi, T., Hara, H., Tsuneta, S., & Ogawara, Y. 1994, Nature, 371, 495

Mazzotta, P., Mazzitelli, G., Colafrancesco, S., & Vittorio, N. 1998, A&AS, 133, 403

McTiernan, J. M., Fisher, G. H., & Li, Peng 1999, ApJ, 514, 472

Mewe, R., Gronenschild, E. H. B. M., & van den Oord, G. H. J. 1985, AAS, 62, 197

Mewe, R., Lemen, J. R., Peres, G., Schrijver, J., & Serio, S. 1985, A&A, 152, 229

Meyer, J.-P. 1985, ApJS, 57, 173

Neupert, W. M., & Swartz, M. 1970, ApJ, 160, L189

Parmar, A. N., Culhane, J. L., Rapley, C. G., Antonucci, E., Gabriel, A. H., & Loulergue, M. 1981, MNRAS, 197, 29P

Parmar, A. N., Culhane, J. L., Rapley, C. G., Wolfson, C. J., Acton, L. W., Phillips, K. J. H., Dennis, B. R. 1984, ApJ, 279, 866

Phillips, K. J. H., Bhatia, A. K., Mason, H. E., & Zarro, D. M., 1996. ApJ, 466, 549

Phillips, K. J. H., Lemen, J. R., Cowan, R. D., Doschek, G. A., & Leibacher, J. W. 1983, ApJ, 265, 1120

Phillips, K. J. H., Neupert, W. M., & Thomas, R. J. 1974, Sol. Phys., 36, 383

Phillips, K. J. H. & Neupert, W.M., 1973. Sol. Phys., 32, 209

Phillips, K. J. H., Pike, C. D., Lang, J., Watanabe, T., & Takahashi, M. 1994, ApJ, 435, 888

Phillips, K. J. H., Rainnie, J. A., Harra, L. K., Dubau, J., Keenan, F. P., & Peacock, N. 2003, A&A (submitted)

Phillips, K. J. H., Sylwester, J., Sylwester, B., & Landi, E., 2003b, ApJL, 589, L113

Sevier, K. D. 1979, ADNDT, 24, 323

Spitzer, L. 1962, Physics of Fully Ionized Gases, John Wiley: New York

Starr, R. et al. 2000, Icarus, 147, 498

Sylwester, J., Culhane, J. L., Doschek, G. A., Oraevsky, V. N., Phillips, K. J. H., and Sylwester, B. 2002, Proc. European Solar Physics Meeting, ESA SP-506, 765

Sylwester, J., Lemen, J. R., & Mewe, R. 1984, Nature, 310, 665

Tanaka, K. 1986, PASJ, 38, 225

Yoshimori, M. et al. 1991, Sol. Phys., 136, 69

This manuscript was prepared with the AAS LaTeX macros v5.0.

From: "Kenneth Phillips" <phillips@stars.gsfc.nasa.gov>
To: <Kristine.D.Glass@nasa.gov>
Cc: <Brian.R.Dennis@nasa.gov>, <phillips@stars.gsfc.nasa.gov>
Subject: Paper on Solar Flare X-ray Emission
Date: Fri, 22 Aug 2003 11:52:25 -0400
Organization: RHESSI group
X-Mailer: Microsoft Outlook, Build 10.0.3416
Importance: Normal

Paper for Astrophysical Journal:

Author: K. J. H. Phillips

Abstract: The 4--10 keV solar flare spectrum includes highly excited lines of stripped Ca, Fe, and Ni ions as well as a continuum steeply falling with energy. Groups of lines at 7~keV and 8~keV, observed during flares by the broad-band {\it RHESSI} spectrometer and called here the Fe-line and Fe/Ni-line features, are formed mostly of Fe lines but with Ni lines contributing to the 8~keV feature. Possible temperature indicators of these line features are discussed -- the peak or centroid energies of the Fe-line feature, the line ratio of the Fe-line to the Fe/Ni-line features, and the equivalent width of the Fe-line feature. The equivalent width is by far the most sensitive to temperature. However, results will be confused if, as is commonly believed, the abundance of Fe varies from flare to flare, even during the course of a single flare. With temperature determined from the thermal continuum, the Fe-line feature becomes a diagnostic of the Fe abundance in flare plasmas. These results are of interest for other hot plasmas in coronal ionization equilibrium such as stellar flare plasmas, hot gas in galaxies, and older supernova remnants.

Let me know if there's anything more you want.

Ken

Ken Phillips
NRC Senior Research Associate
NASA/Goddard Space Flight Center
Code 682 (Bldg. 21, RHESSI)
Greenbelt, MD 20771
USA
Phone +1 301 286 1758
FAX + 1 301 286 1617
Email phillips@stars.gsfc.nasa.gov